Journal of Advanced Engineering Trends
ISSN : 2682 - 2091

Vol. 44, No. 1, January 2025

Numerical Calibration for Torsional Retrofitting of RC Beams with Near Surface Mounted (NSM) Continuous Spiral Reinforcement

Serageldin A. T. Hassouna[1,*], Alaa Eldein Y. Abouelezz[1]
[1] *Civil Engineering Dep., Faculty of Engineering, Minia University, Minia, Egypt*
** Corresponding author(s) E-mail: serag.hassouna@gmail.com*

A R T I C L E I N F O

Article history:
Received: 2 September 2024
Accepted: 16 February 2024
Online: 3 March 2025

Keywords:
Near Surface Mounted (NSM),
Spiral, Continuous, Torsional capacity,
RC beams,
ANSYS,
Drucker-Prager,
Hardening, Softening, Dilatation (HSD)

A B S T R A C T

Near surface mounted (NSM) technique has become one of the most prominent methods in retrofitting and strengthening structural elements. Literature does not provide a systematic and clear way to model the material of RC beams under combined torsion and bending loading, and is mostly experimental. A calibration procedure was carried out using the nonlinear finite element analysis program "ANSYS" in order to provide such a way of modeling.
The experimental RC beams specimens upon which the calibration process is applied are deficient in stirrups and with no side bars, hence the control beam specimen is deficient in torsional capacity, this is to provide room for torsional retrofitting. This study focuses on the needed rationale and parametric values to model concrete retrofitted with NSM continuous rectangular spiral reinforcement using Drucker-Prager Concrete material model combined with hardening, softening and dilatation (HSD) exponential material model, to be provided in order to reach good numerical results.

1. Introduction

Torsional loading is considered one of the most critical design and strengthening loading types for reinforced concrete beams. The interconnection between reinforcement and concrete was identified in order to understand the torsional mechanisms [1-3], with the focus mainly on analytical models such as the work of (Hsu and Mo, 2010) [4].

The nature of studying near surface mounted applications (as a retrofitting method) is mostly experimental through literature. The following are some recent notable research from the literature on NSM under torsional loading, whether pure or combined with bending. (Al-Bayati 2018) [5] carried out experiments under pure torsion on beams retrofitted with NSM Carbon Fiber Reinforced Polymer (CFRP) laminates and ropes with different configurations and groove filling materials.

(Askander and Mahmood 2020a)[6] applied NSM strengthening using steel bars with different spacing values and with 90 ˚and 45 ˚ angles on inclination. This is under combined torsion and bending. (Alrawi and Mahmood 2022) [7] carried out finite element analysis (FEA) under pure torsion with reinforced concrete rectangular beams strengthened with CFRP bars on the sides of the beam and NSM steel bars in ring shape with different spacing values.

This work used the conventional modeling of the materials in ANSYS based on the work of (Kachlakev et al, 2001) [8] and with the use of SOLID65 to model concrete elements, LINK180 to model steel bars, SHELL41 to model CFRP bars and SOLID185 to model bearing plates. Moreover, recent research using finite element analysis software to study strengthening or the new reinforcement arrangement in RC beams were carried out.

(Rana et al, 2024) [9] examined using ABAQUS, a finite element analysis software, the strengthening of RC frame connection using two methods, steel plates and RC blocks, both applied externally. Concluding the optimum steel plate thickness to be 6 mm, and the degrees of resistance enhancement when the application of the strengthening object is in the tension zone only or in both the tension and compression zone.

(Thaer et al, 2023) [10] examined with the use of ANSYS finite element analysis software the behavior of RC beams under pure torsion, with different transverse reinforcement configurations, which are the traditional vertical closed stirrups, the circular spiral stirrups and the inclined rectangular spiral stirrups. (Yasser et al, 2022) [11] studied under flexural loading reinforcing beams additionally with mild steel plates experimentally, then conducted verification and parametric study upon the reinforcement plates using ANSYS.

2. Experimental Work Summary

Research on the geometrical configuration of transverse reinforcement confirmed that the best torsional performance is when using continuous spiral reinforcement along the beam length in the locking direction [12-14]. Hence, the idea of the experimental work from which this numerical study is calibrated. (Askander and Mahmood 2020b) [15] applied NSM using steel wire ropes of diameter 8 mm configured with continuous rectangular spiral manner, under combined torsion and bending loading. The schematic of setting up the test on the specimens is illustrated in Fig.1. The dimensions and internal reinforcement are shown on Fig.2. Five spacing values were made using equal divisions of the longitudinal pitch length (800 mm), this is illustrated in Fig.4.

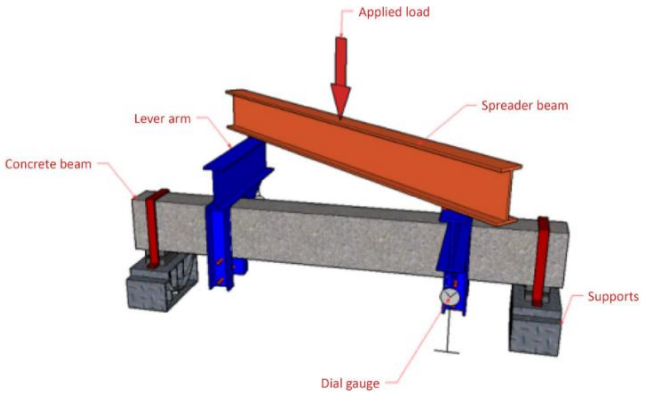

Figure 1: Schematic of Setup of the Test (Experimental Work) [15]

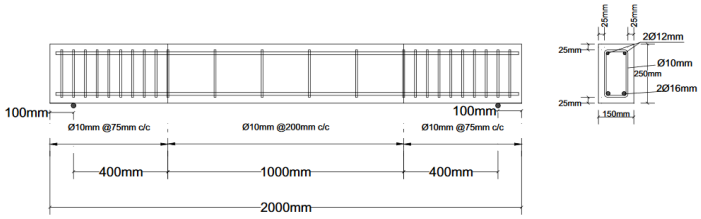

Figure 2: Dimensions and Internal Reinforcement Details (Experimental Work) [15]

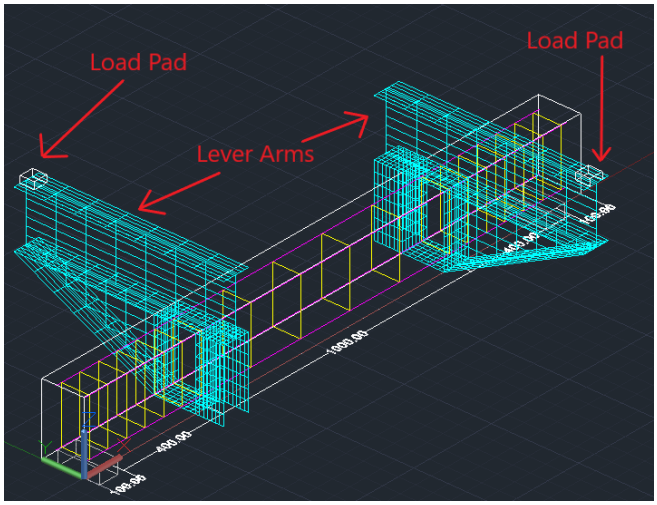

Figure 3: Idealized geometry and longitudinal spans in between loading arms and supports on the concrete beam

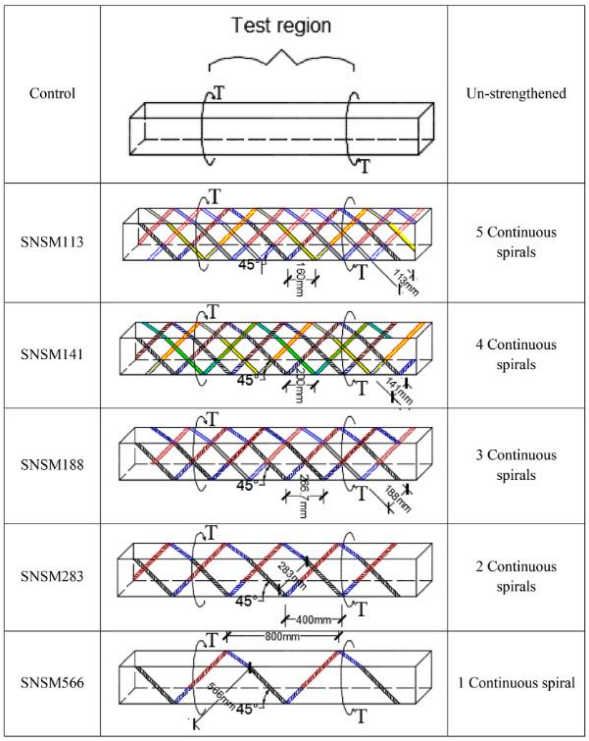

Figure 4: Steel Wire Ropes Configuration (Experimental Work) [15]

3. Idealization, Meshing and Element Types

Fig.3 shows the longitudinal spans and the idealized geometry of the elements except for the NSM reinforcement. Load pads replace the spreader beam, and take the torsional loads at the end of each lever arm. This is done in order to reduce the time of meshing and running the analysis every time. Fig.7 and Fig.8 illustrate the idealized geometries and meshing for all models.

Automatic meshing is chosen manually to default with 25 mm as maximum and regular mesh size. Steel plates of the lever arms of thickness 8 mm[15] are modeled with SHELL181 elements with four nodes, where every node has the conventional six degrees of freedom for translation and rotation [16]. Then are bonded using "Contact Region" feature, to fully bond them to each other.

Reinforcement rebars and NSM continuous spiral wire ropes are modeled using MESH200 element type with KEYOPT(1)=2, which is a 3D line with two nodes [16]. Then to be automatically converted into REINF264 3D line spars which are embedded within the concrete "base elements" [16]. It is worth noting that no interface elements between reinforcement and concrete are implemented here, this is in order to fully utilize them with no debonding aftereffects.

Concrete elements are modeled using SOLID185, the same element type for the supports and load pads. This is because ANSYS does not support the use of SOLID65 for base elements with REINF264 reinforcement elements [16]. Values of spacing and simplified symbols for every specimen and its correspondent FEA model are provided in Table 1.

4. Boundary Conditions

In order to capture both the effect of torsional loading purely and the other component of the bending effect, virtual superposition is implemented. Fig.5 represents the virtual superposition of flexural and torsional loads (which are indeed virtual in the nature of this 3D modeling and are singular in effect in reality). Fig.6 illustrates how the boundary conditions are applied onto the idealized geometry before meshing.

The relation between the torsional load (F_{Tu}) and the flexural load (F_{Mu}) is

$$F_{Mu} = 1.15\ F_{Tu}$$

which is discovered from the experimental capacities illustrated in Table 2. Then, to get the torsional load from the support reaction from the model's solution

$$F_{Tu} = \text{Support reaction in Z direction} \div 2.15$$

Hence, there is no real load duplication.

Table 1: Spacing Values and Their Correspondent Specimen Adopted Symbols

Beam [15]	Simplified Symbol	Spacing (mm)
Control	Control	∞
SNSM566	S1	566
SNSM283	S2	283
SNSM188	S3	188
SNSM141	S4	141
SNSM113	S5	113

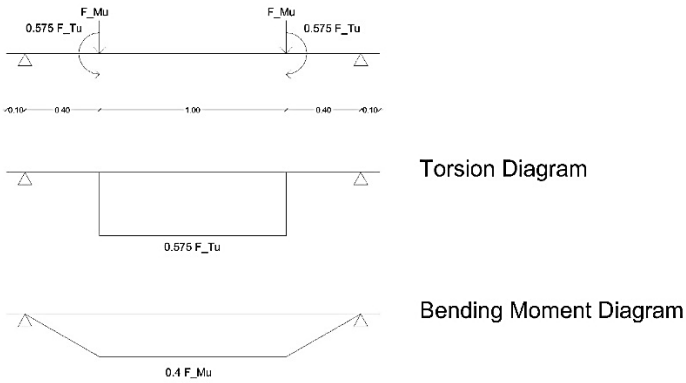

Figure 5: Diagrams of Torsion and Bending Applied on the Beam in Virtual Superposition

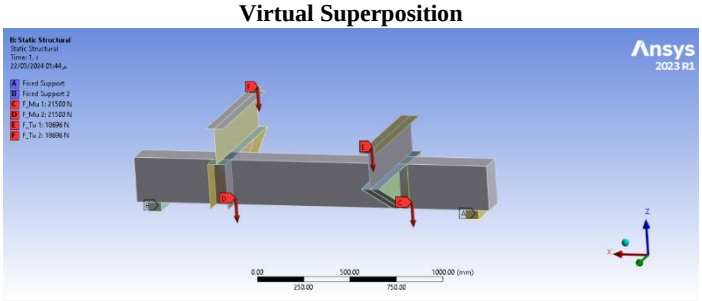

Figure 6: Applied Boundary Conditions of the Control Beam

Table 2: Experimental Ultimate Torsional and Flexural Capacities

Beam	M_u (KN.m) [15]	T_u (KN.m) [15]	F_{Tu} (KN)	F_{Mu} (KN)	F_{Mu}/F_{Tu}	$F_{Mu} + F_{Tu}$
Control	8.6	10.75	18.70	21.5	1.15	40.20
S1	10.06	12.58	21.88	25.15	1.15	47.03
S2	12.62	15.78	27.44	31.55	1.15	58.99
S3	14.32	17.9	31.13	35.8	1.15	66.93
S4	18.2	22.75	39.57	45.5	1.15	85.07
S5	20.6	25.75	44.78	51.5	1.15	96.28

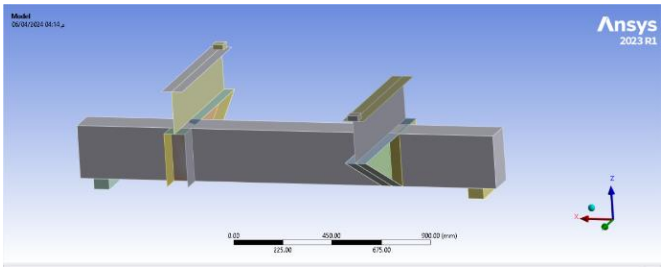

(a) Control Beam Model Geometry

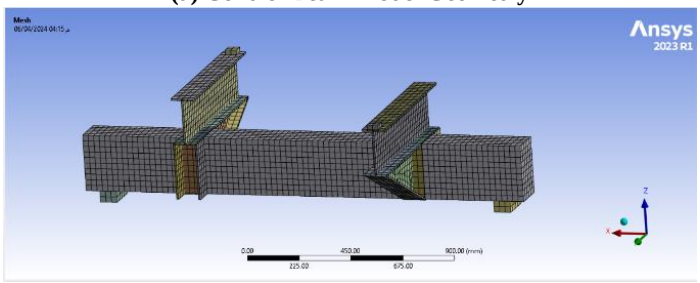

(b) Control Beam Model Mesh

Figure 7: Geometrical Idealization and Meshing of Control Beam

The idea of this superposition emerged from the case of sole application of the loads at the end of each lever arm, i.e. torsional loads. The result at this case was the absence of flexural deformation, most notably the mid-span deflection. Hence, flexural loads are needed (specifically for this 3D modeling case) to get the effect of flexural deformation.

5. Solution Settings

In order to make the loading increment for all of the models almost the same, the number of substeps for control beam is initially chosen (here is chosen to be 200), and F_{Mu} for it is picked close to or equal to the experimental value (here is chosen to be equal to the experimental result which is 21500 N). Then the other substeps are calculated maintaining the ratio between substeps and their correspondent F_{Mu} a constant value (here is calculated to equal to 107.5 N/# substeps), then a closer number of substeps is chosen for the other models, then the applied virtual end flexural and torsional loads are updated maintaining the same ratio between F_{Mu} and number of substeps. The result of this process is represented in Table 3.

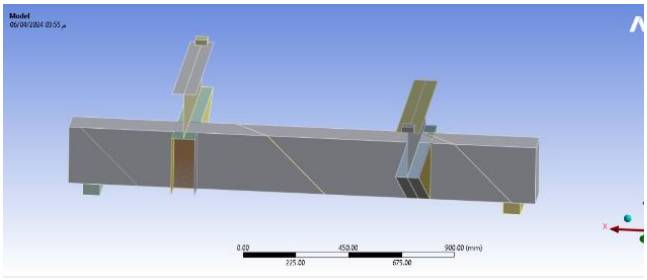

(a) S1 Beam Model Geometry

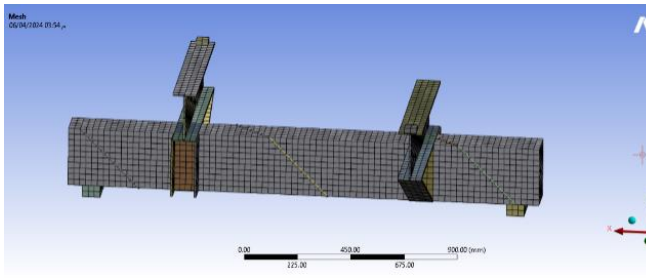

(b) S1 Beam Model Mesh

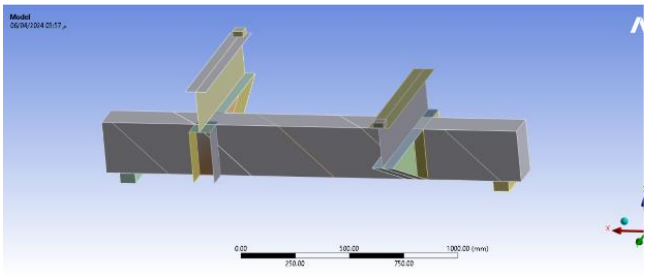

(c) S2 Beam Model Geometry

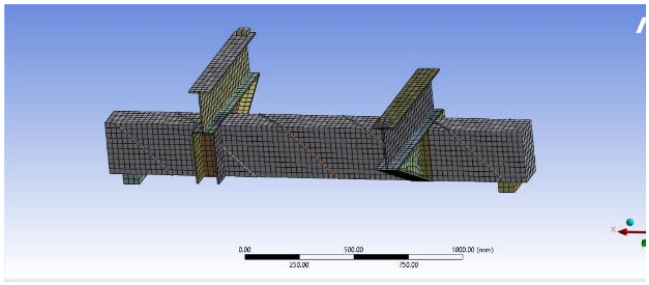

(d) S2 Beam Model Mesh

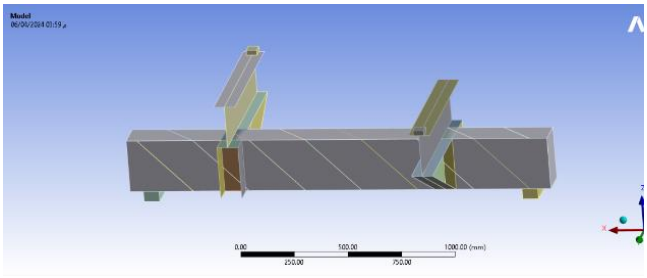

(e) S3 Beam Model Geometry

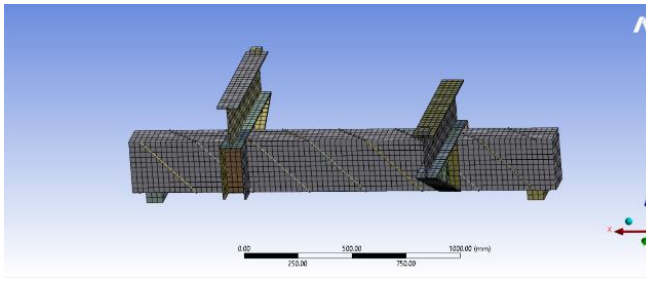

(f) S3 Beam Model Mesh

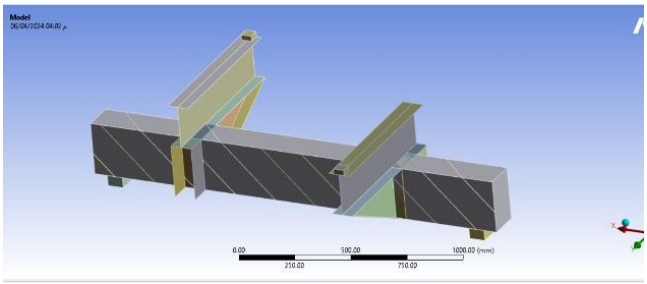

(g) S4 Beam Model Geometry

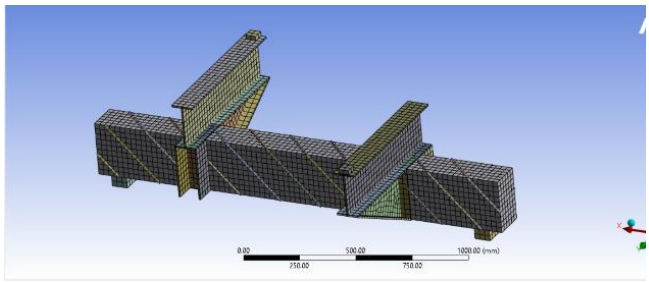

(h) S4 Beam Model Mesh

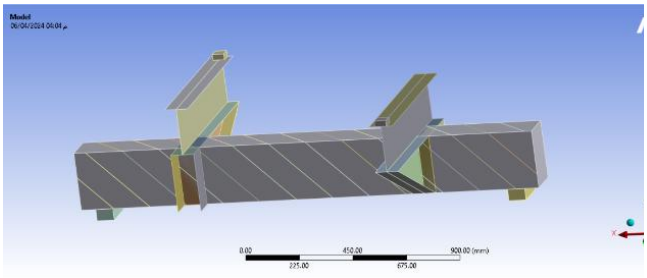

(i) S5 Beam Model Geometry

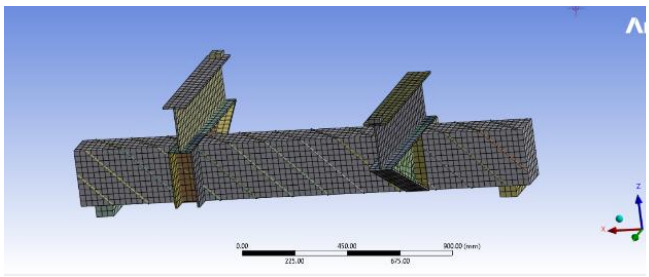

(k) S5 Beam Model Mesh

Figure 8: Geometrical Idealization and Meshing of Beams from S1 to S5

Table 3: Applied Number of Substeps, Torsional and Flexural Loads within the models

Beam	# substeps (not rounded)	# substeps chosen	F_{Tu} chosen (N)	F_{Mu} chosen (N)
Control	200	200	18696	21500
S1	234	240	22435	25800
S2	293.53	300	28044	32250
S3	333.02	340	31783	36550
S4	423.26	430	40196	46225
S5	479.07	490	45804	52675

6. Material Models

6.1. Reinforcement, Supports, Lever Arms and Load Pads

All these elements are modeled as bilinear isotropic, and all of them have Poisson's ratio equal 0.30. Supports, lever arms and load pads are given higher values to behave as stiff elements, compared to both concrete and reinforcement, whether this reinforcement is internal or NSM, with modulus of elasticity equals to 2E+6 GPa and tangent modulus 100 MPa. Internal reinforcement and NSM steel wire ropes have the same modulus of elasticity, which equals 2E+5 MPa. Internal reinforcement have the conventional yield strength of 540 MPa, and NSM steel wire ropes have yield strength of 700 MPa. Much close to the experimental report values of 541 MPa and 702 MPa respectively [15].

6.2. Concrete

6.2.1 Linear Isotropic Parameters

Modulus of elasticity (E_c) is taken according to ACI-318M [18] with degradation 5% to coincide with the elastic stage.

$$E_c = 0.95 * 4700\sqrt{f_c} \text{ in MPa}$$

As the experimental compressive strength is 48 MPa [15], the concrete modulus of elasticity is 30848 MPa. Poisson's ratio of concrete is taken to be 0.20.

6.2.2. Drucker-Prager Concrete Material Model

Five Parameters need to be defined in this material model, three for the strength of concrete in tension and compression, and two dilatancy parameters also related to tension and compression of concrete. The symbols and ranges of them are illustrated in Table 4. The dilatancy parameters are set to 1.0 in order to represent concrete in an ideal state of no change in volume.

The compressive and tensile strength parameters are chosen to be set in almost equal values, which are proportions of the actual experimental compressive strength. Their values for each model are illustrated in Table 6, and their percentages of the experimental compressive strength are illustrated in Table 7. The reason for this choice is to get the torque-twist curves to come close to the experimental ones. Moreover, the chosen value gets a little higher with the decrease of spacing to represent the increase of confinement.

Table 4: Drucker-Prager Concrete Parameters Definition [17]

Parameter	Symbol	Range
Uniaxial compressive strength	f_{cu}	$f_{cu} > f_t$
Uniaxial tensile strength	f_t	$f_t > 0$
Biaxial compressive strength	f_{cbi}	$f_{cbi} > f_{cu}$
Tensile and tension-compression dilatancy	δ_t	$0 < \delta_t \leq 1$
Compression dilatancy	δ_c	$0 < \delta_c \leq 1$

Table 5: Exponential HSD Parameters Symbols and Ranges [17]

Parameter	Symbol	Range
Plastic strain at uniaxial compressive strength	κ_{cm}	$0 < \kappa_{cm} \leq 0.02$
Plastic strain at transition from power law to exponential softening	κ_{cu}	$\kappa_{cu} > \kappa_{cm}$
Relative stress at start of nonlinear hardening	Ω_{ci}	$0 \leq \Omega_{ci} \leq 1$
Residual relative stress at κ_{cu}	Ω_{cu}	$\Omega_{cr} < \Omega_{ci} \leq 1$
Residual compressive relative strength	Ω_{cr}	$0 < \Omega_{cr} < \Omega_{cu}$
Mode I area-specific fracture energy	G_{ft}	$G_{ft} > 0$
Residual tensile relative strength	Ω_{tr}	$0 < \Omega_{tr} \leq 1$

Table 6: Drucker-Prager Concrete Parameters Definition within models

Beam	f_{cu} (MPa)	f_t (MPa)	f_{cbi} (MPa)
Control	4.8	4.79	4.81
S1	5.82	5.81	5.83
S2	5.8	5.79	5.81
S3	5.8	5.79	5.81
S4	7.2	7.19	7.21
S5	8.5	8.49	8.51

Table 7: Drucker-Prager Concrete Parameters Percentage Relative to the Experimental Uniaxial Compressive Strength

Beam	f_{cu}/f_c %	f_t/f_c %	f_{cbi}/f_c %
Control	10.00%	9.98%	10.02%
S1	12.13%	12.10%	12.15%
S2	12.08%	12.06%	12.10%
S3	12.08%	12.06%	12.10%
S4	15.00%	14.98%	15.02%
S5	17.71%	17.69%	17.73%

6.2.3. Hardening, Softening and Dilatation (HSD) Exponential Material Model

This material model is chosen to represent the degradation of the concrete performance during loading. If not used the torque-twist curves will be linear with slope equal to the initial concrete modulus of elasticity until the end of the FEA session. In addition, substitution of the actual compressive and tensile uniaxial and biaxial strength values result in the same over stiffness of concrete.

In summary, a degraded concrete combined with HSD exponential material model is the strategy to get the numerical results close to the experimental ones. The needed parameters and their ranges are illustrated in Table 5, and their chosen values in Table 8, while Fig.9 represents graphically the contribution of

these parameters into the softening functions of this material model under tension and compression.

6.2.3.1 κ_{cm}

This parameter is found to provide the ductile behavior for the finite element analysis. The proposed values are close or equal to the maximum allowable value from ANSYS, as illustrated in Table 5. Hence, the choice of 0.02 is recommended.

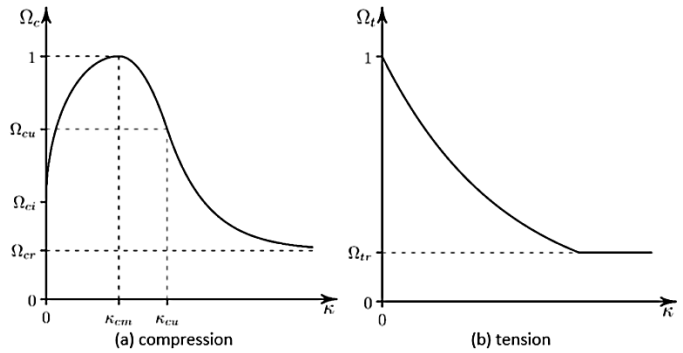

Figure 9: Exponential Softening in Compression and Tension [17]

Table 8: Exponential HSD Parameters Definition within models

Beam	κ_{cm}	κ_{cu}	Ω_{ci}	Ω_{cu}	Ω_{cr}	G_{ft} (N/mm)	Ω_{tr}
Control	**0.015**	**0.105**	**0.2**	**0.2**	**0.05**	**90000**	**0.05**
S1	**0.02**	**100**	**0.2**	**1**	**0.99**	**1.00E+20**	**0.05**
S2	**0.02**	**100**	**0.3**	**1**	**0.99**	**1.00E+20**	**0.05**
S3	**0.02**	**100**	**0.3**	**1**	**0.99**	**1.00E+20**	**0.05**
S4	**0.02**	**100**	**0.3**	**1**	**0.99**	**1.00E+20**	**0.05**
S5	**0.02**	**100**	**0.3**	**1**	**0.99**	**1.00E+20**	**0.05**

6.2.3.2 κ_{cu}

This parameter is found to be beyond the reach of the FEA session, this is because the models when contain forces in their boundary conditions lose convergence before the start of softening stage, i.e. the stage at which decreasing of load is accompanied with increasing of deformation. In other words, the concrete deforms in two stages, an elastic stage then a hardening plastic stage. The only concern for this parameter is to be substituted with a value bigger than κ_{cm}.

6.2.3.3 Ω_{ci}

This parameter represents the proportion of compressive strength at which the HSD material model starts to affect the analysis. About 20% to 30% is found to be suitable choice, mainly to affect the confinement behavior in the torque-twist graphs.

6.2.3.4 Ω_{cu} *and* Ω_{cr}

The same as with κ_{cu}, they belong to the softening stage where the solution of the model fails to converge. The choice of their values for the control beam is according to the recommendations of (Dmitriev et al. 2020) [19]. Then, after the realization of their insignificant role, the simplified values of 0.99 and 1.0 are chosen.

6.2.3.5. G_{ft}

(Dmitriev et al. 2020) [19] proposed the recommendation for the choice of this parameter. The control model value of 90 N/m comes from this recommendation from Fig.10. The choice of a numerical bigger value for the other models (here is set to be 1.00E+20 N/mm) is in order to make the loss of convergence as far as possible, with no effect on the solution results themselves.

6.2.3.3 Ω_{cr}

This value is also proposed by (Dmitriev et al. 2020)[19] and is taken as is, with no change or modification.

Max. aggregate size d_{max}, mm	G_{ft0}, N×m/m^2	G_{ft}, N×m/m^2			
		C20	C40	C60	C80
8	25	50	70	95	115
16	30	60	90	115	135
32	58	80	115	145	175

Figure 10: Fracture Energy Values for Different Concrete Grades (Dmitriev et al, 2020) [19]

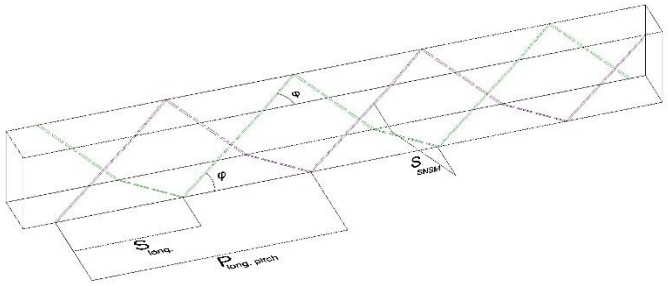

Figure 11: Schematic of the Continuous Spiral NSM Reinforcement

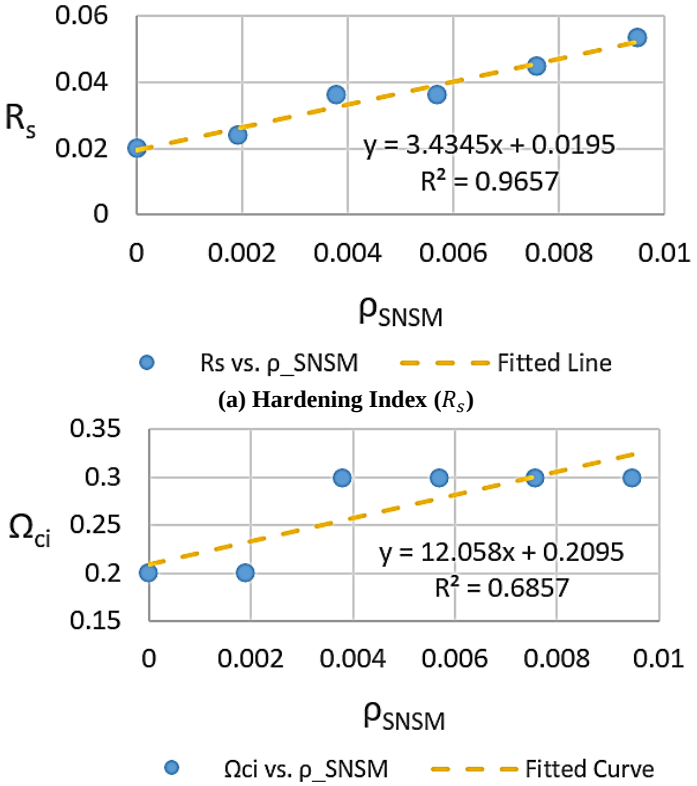

(a) Hardening Index (R_s)

(b) Relative stress at start of nonlinear hardening (Ω_{ci})

Figure 12: NSM Volumetric Ratio Relation with R_s and Ω_{ci}

7. Gauging the NSM Confinement

Two main parameters are used to gauge the confinement of specimens.

1. NSM Volumetric Ratio (ρ_{SNSM})
2. Hardening Index (R_s)

NSM volumetric ratio is the volume of the NSM steel wire ropes in the unit volume of the concrete, and is calculated from the following expression.

$$\rho_{SNSM} = \frac{2(b+d)\,A_{ss}}{b\,d\,S_{SNSM}}$$

where

$$S_{SNSM} = S_{long.} \sin\varphi$$

The general geometrical schematic of continuous spiral NSM reinforcement is illustrated in Fig.11. Hardening index is defined as the following expression.

$$R_s = \Omega_{ci} \frac{f_{cu}}{f_c}$$

where f_c is the experimental compressive strength. This parameter provides a dimensionless estimate about the degree of confinement of NSM.

8. Results

8.1. First Elastic Torque

From Table 8 it shows that setting the number of substeps adhering to the described methodology in clause 5 results into that the loading increments for all the models are almost the same.

8.2. Deformation Overview

From {Fig.13, Fig.14, Fig.15, Fig.16, Fig.17, Fig.18} the flexural and twist deformation appearance lead to conformity with the loading type of combined torsional and bending effect. The twist is vividly clear and is accompanied with mid-span deflection ranging from around 5 mm to 10 mm, close enough to the reported range of values in the experimental work, which is from around 3 mm to 9 mm.

8.3. Torque-Twist Verification Graphs

From Fig.21 FEA results show less ductile behavior than the experimental ones, with the ultimate torque deviation ranging from -10.50% to -17.64%, as mentioned in Table 9. This means that the FEA results (based on the previously proposed parametric values) are within the practical bounds of the experimental ones, though they show less ductility and load carrying capacity, i.e. underestimation, though the parameter κ_{cm}, which is responsible for the ductility of numerical FEA models is set close to or equal to its maximum allowable value.

Table 8: First Elastic Torque

Beam	1st Elastic Torque (N)
Control	53.75
S1	53.74
S2	53.77
S3	53.75
S4	53.76
S5	53.71

Table 9: Torque-Twist Experimental vs. Finite Element Models Results

Beam	T_u Exp (KN.m) [15]	T_u FEA (KN.m)	T_u deviation%
Control	10750	9621.22	-10.50%
S1	12580	10829.52	-13.91%
S2	15780	14140.99	-10.39%
S3	17900	15860.91	-11.39%
S4	22750	19294.59	-15.19%
S5	25750	21208.41	-17.64%

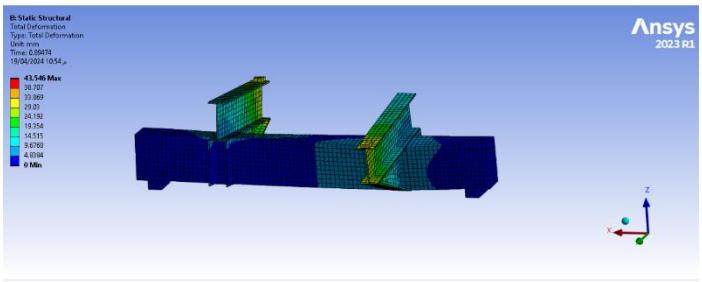

Figure 13: Control Beam Deformed Shape

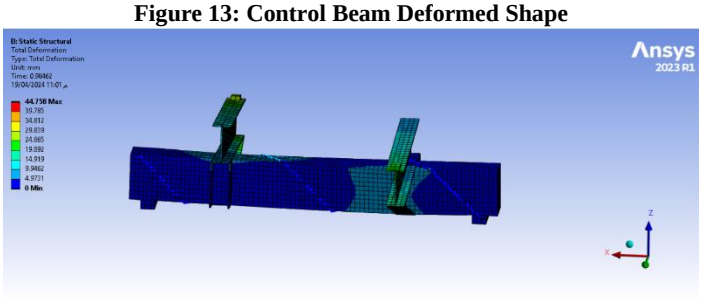

Figure 14: S1 Beam Deformed Shape

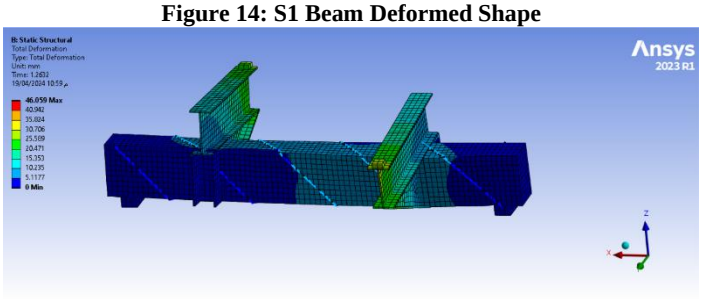

Figure 15: S2 Beam Deformed Shape

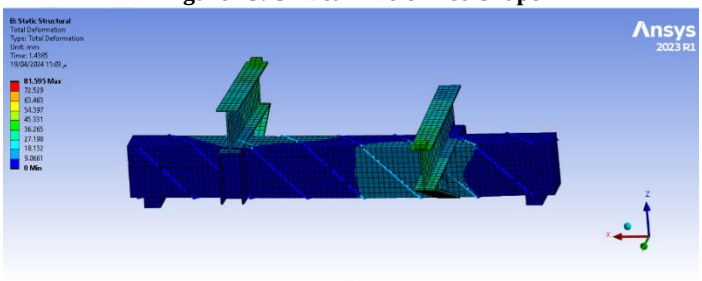

Figure 16: S3 Beam Deformed Shape

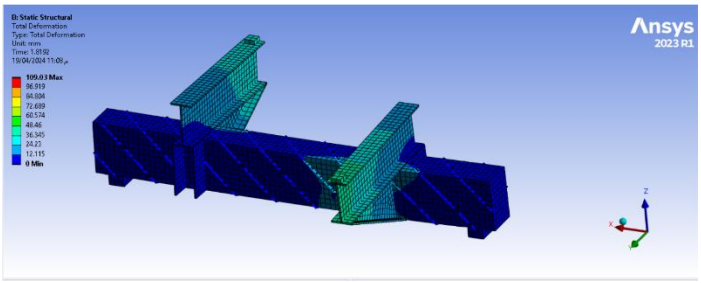

Figure 17: S4 Beam Deformed Shape

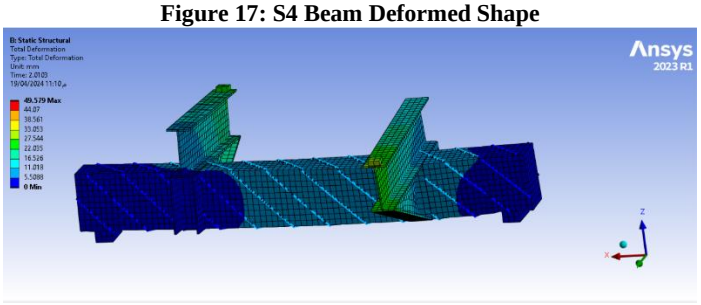

Figure 18: S5 Beam Deformed Shape

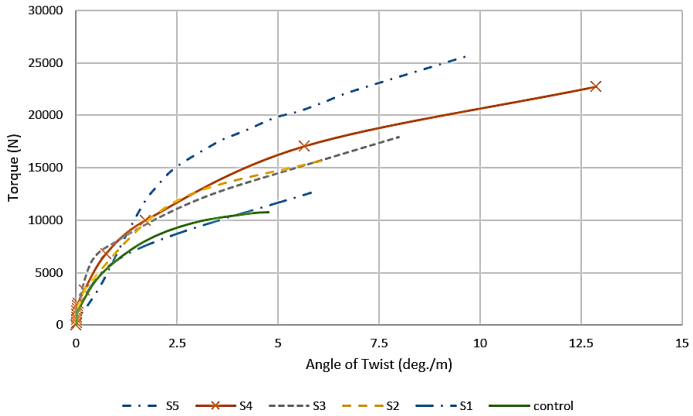

Figure 19: Torque vs. Angle of Twist (Experimental Results) [15]

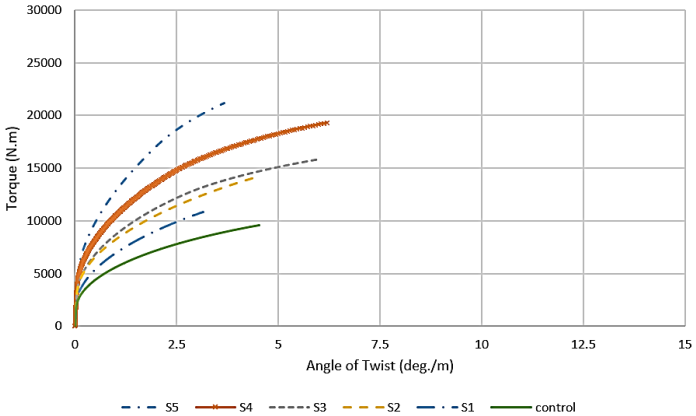

Figure 20: Torque vs. Angle of Twist (FEA Results)

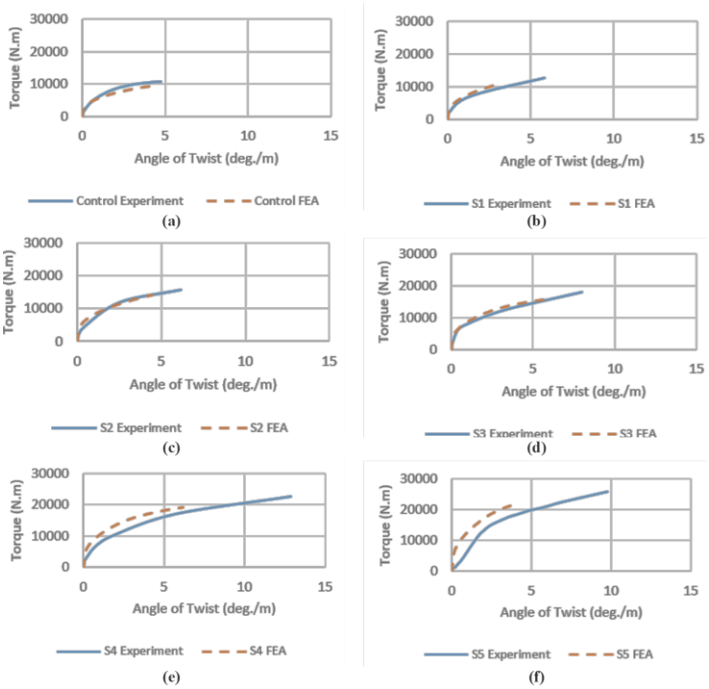

Figure 21: Torque-Twist Experiment vs. FEA (All Beams)

9. Conclusions

1. RC rectangular beams retrofitted with NSM continuous rectangular spiral reinforcement under combined torsional and bending loading, a new modeling scheme for concrete other than stress-strain relations is proposed to yield the results within the experimental practical bounds of torque and twist.
2. Drucker-Prager concrete material model compression and tension parameters need to be substituted with a proportion of the actual characteristic compressive strength, about 10% for the unconfined (control) beam, with slight increase for the proceeding models; this is to match with the actual increase of confinement.
3. Compressive and tensile dilatation are set to 1.0 to represent the absence of volumetric change.
4. The HSD parameters set $\{\kappa_{cu}, \Omega_{cu}, \Omega_{cr}\}$ are beyond the scope of the analysis, this is because the FEA solution does not converge in the softening stage, if the supplied boundary conditions contain forces, and these parameters work mainly in the softening stage.
5. Hardening Index set of values represent numerically the degrees of confinement for a given set of experiments to be calibrated. Strong linear trend correlation with respect to NSM volumetric ratio must be achieved.

Nomenclature

A_{ss}	cross-section area of the NSM reinforcement.
b	breadth of the beam rectangular section.
d	depth of the beam rectangular section.
E_c	Concrete modulus of elasticity.
f_c	Experimental uniaxial compressive strength.
f_{cu}	Numerical uniaxial compressive strength.

f_t	Numerical uniaxial tensile strength.
f_{cbi}	Numerical biaxial compressive strength.
F_{Tu}	Torsional load.
F_{Mu}	Flexural load.
G_{ft}	Mode I area-specific fracture energy.
M_u	Ultimate moment.
$P_{long.\ pitch}$	NSM reinforcement pitch length in the longitudinal direction (see Fig.11).
R_s	Hardening Index.
$S_{long.}$	Spacing of the NSM reinforcement, in the longitudinal direction (see Fig.11).
S_{SNSM}	Spacing of the NSM reinforcement, in the perpendicular direction of the angle of inclination (see Fig.11).
T_u	Ultimate torque.
φ	Angle of inclination of NSM from the beam's longitudinal direction (see Fig.11).
ρ_{SNSM}	NSM volumetric ratio.
δ_t	Tensile and tension-compression dilatancy.
δ_c	Compression dilatancy.

Conflict of Interest

The authors declare no conflict of interest.

References

1. Hsu, T.T.C., *Torsion of structural concrete—plain concrete rectangular sections.* ACI Journal Proceedings, 1984. **81**(1): p. 11-18.
2. Hsu, T.T.C. and Y.L. Mo, *Softened truss model theory for shear and torsion.* ACI Structural Journal, 1985. **82**(2): p. 219-231.
3. Hsu, T.T.C., *Shear Flow Zone in Torsion of Reinforced Concrete.* Journal of Structural Engineering, 1990. **116**(11): p. 3206-3226.
4. Hsu, T.T.C. and Y.L. Mo, *Unified Theory of Concrete Structures*. 2010: John Wiley & Sons.
5. Bayati, G.A., *Torsional Strength Enhancement of Reinforced Concrete Beams with Near Surface Mounted Carbon Fibre Reinforced Polymer Composites*, in *FACULTY OF SCIENCE, ENGINEERING AND TECHNOLOGY*. 2018, SWINBURNE UNIVERSITY OF TECHNOLOGY.
6. Askandar, N.H. and A.D. Mahmood, *Torsional Strengthening of RC Beams with Near-Surface Mounted Steel Bars.* Hindawi, Advances in Materials Science and Engineering, 2020. **2020**.
7. Alrawi, M.A. and M.N. .Mahmood, *Strengthening Reinforced Beams Subjected to Pure Torsion by Near Surface Mounted Rebars.* Anbar Journal of Engineering Science (AJES), 2022. **12**(1): p. 13-22.
8. Kachlakev, D., et al., *Finite Element Modeling of Reinforced Concrete Structures Strengthened with FRP Laminates*. 2001.
9. Mohsen, R.M., A. Abouelezz, and R.A. Sadeek, *A Numerical Study of Strengthening the External RC Frame Connection with Steel Plates and RC Blocks.* Journal of Advanced Engineering Trends, 2024. **43**(2): p. 347-368.
10. Mohammed, T.J., K.M. Breesem, and A.F. Hussein, *Numerical Analysis of Torsional Reinforcement of Concrete Beams in Unconventional by ANSYS Software.* Civil Engineering Journal, 2023. **9**(1): p. 41-51.
11. Tawfic, Y.R., A.-N.A. Soltan, and A.B. Saddek, *Characteristics of Steel Plate-Reinforced Concrete Composite Beams Subjected to Flexural Stresses.* Journal of Advanced Engineering Trends, 2022. **41**(2): p. 41-53.
12. Chalioris, C.E. and C.G. Karayannis, *Experimental investigation of RC beams with rectangular spiral reinforcement in torsion.* Engineering Structures, 2013. **56**: p. 286-297.
13. Katkhuda, H.N., N.K. Shatarat, and A.A. AL-Rakhameen, *Improving the Torsional Capacity of Reinforced Concrete Beams with Spiral Reinforcement.* International Journal of Structural and Civil Engineering Research 2019. **8**(2): p. 113-118.
14. Mahmoud, S., A. Youssef, and H. Salem, *Enhanced Torsion Mechanism of Small-Scale Reinforced Concrete Beams with Spiral Transverse Reinforcement.* Civil Engineering Journal, 2022. **8**(11): p. 2640-2660.
15. Askandar, N.H. and A.D. Mahmood, *Torsional Strengthening of RC Beams with Continuous Spiral Near-Surface Mounted Steel Wire Rope.* International Journal of Concrete Structures and Materials, 2020. **14**(7): p. 1-16.
16. ANSYS Inc., *ANSYS Mechanical APDL Element Reference for Release 18.2*. 2017.
18. ACI Committee 318, *ACI 318M-14*. 2014.
19. Dmitriev, A., et al., *Calibration and Validation of the Menetrey-Willam Constitutive Model for Concrete*. Construction of Unique Buildings and Structures, 2020. **88**.